06

High-frequency magnetron sputtering and morphological properties of carbon nanowalls

© A.Ya. Vinogradov,[1] S.A. Grudinkin,[1] M.A. Baranov,[2] V.S. Levitskii[3]

[1]Ioffe Institute,
194021 St. Petersburg, Russia
[2]International research and educational center for physics of nanostructures, ITMO University,
199034 St. Petersburg, Russia
[3]R&D Center of Thin Film Technologies in Energetics,
194064 St. Petersburg, Russia
e-mail: grudink.gvg@mail.ioffe.ru

Received October 3, 2024
Revised October 3, 2024
Accepted October 3, 2024

Carbon nanowalls, which are three-dimensional structures made of graphene layers arranged perpendicularly to the substrate surface, were obtained on crystalline silicon substrates using high-frequency magnetron sputtering of a graphite target without the addition of reactive gases to the working mixture. The effect of the deposition process technology on the morphology characteristics of carbon nanowalls and their evolution over growth time was investigated by means of electron microscopy. The structural properties and defects of carbon nanosheets was studied using the method of Raman scattering. The influence of high-frequency energy and argon pressure in the reactor on the content of point and linear structural defects in carbon nanowalls is shown.

Keywords: ion plasma deposition, carbon nanostructures, scanning electron microscopy, Raman light scattering.

DOI: 10.61011/TP.2025.02.60823.305-24

Introduction

Carbon nanowalls (CNW) are curved multilayer graphene plates placed primarily at right angle to the substrate surface. CNW form a three-dimensional structure with high specific surface area to $1000-2000\,m^2/g$ [1] and have high electrical conductivity [2] offering application prospects as components for various electronic devices. CNW feature biocompatibility [3] and, therefore, can be used in medical implantable devices without causing side effects.

Miniaturization trend of modern electronic devices poses a critical task of increasing heat removal efficiency because an increase in heat output density with insufficient heat removal may deteriorate device performance and cause degradation. Graphene layers have high heat conductivity [4,5] and are promising materials for heat removal applications. CNW with a low reflectance of 0.13% [6] may be used as a „black body".

CNW may be also used in supercapacitors, photovoltaic systems, field emission cathodes, gas sensors and biosensors, as catalyst carriers, high-performance radiation absorbers [7] and nanostructure templates [8,9]. Development of photodetectors based on CNW/semiconductor heterostructures is a promising technology area [10].

Several techniques are currently used for making CNW: various plasma-chemical deposition modifications [11–14] that are more often used than others for making CNW; arc discharge [15]; hot filament chemical vapor deposition [16]. Various substrates, including flexible metallic ones, are used for CNW growth. Study of various CNW synthesis techniques in a wide process variable range facilitated understanding the main features of CNW formation.

Most of works use gaseous hydrocarbons and hydrogen as plasma-forming gas for CNW formation. Plasma-forming gas is used for amorphous phase etching and preventing secondary CNW nucleation. These works emphasize that the substrate temperature (450°C and higher), concentration of gaseous hydrocarbon and hydrogen and sometimes of additional catalyst layer on substrate are the key CNW formation factors.

The difference of our approach is in CNW deposition by high-frequency (13.56 MHz) magnetron graphite target glow-discharge plasma sputtering in argon without using catalysts and adding hydrogen and other reactive gases into the plasma-forming mixture. This study uses scanning electron microscopy and Raman scattering spectroscopy methods to investigate the influence of CNW deposition technique and process variables by high-frequency (HF) magnetron graphite target sputtering without using catalysts and reactive gases on the CNW morphology parameters and structure, structural evolution with growth time and features of CNW orientation on structured substrates.

1. Experiment

CNW samples were deposited by magnetron graphite target sputtering in high-frequency (13.56 MHz) discharge current mode in argon without adding reactive gases. The 6516pT (Mersen, France) graphite, diameter 60 mm, was

Table 1. CNW formation process conditions

Sample No.	HF power, W	Argon pressure, Pa	Sputtering time, min	CNW height, nm
1	30	7	50	440
2	30	3	60	520
3	30	3	120	850
4	65	3	35	540
5	100	3	5	–
6	100	3	20	490
7	160	3	10	470

used as the target, the distance between the target and substrate was 70 mm. During film sputtering, the target was cooled with running water.

Film sputtering process variables: substrate temperature 600°C, pressure 1–7 Pa, HF power 30–190 W. Process conditions for making samples to be used for the comparative analysis of CNW properties are listed in Table 1.

Polished KDB-10 (100) single crystal silicon wafers pretreated with chromium mixture (concentrated sulfur acid and potassium dichromate mixture) in an ultrasonic bath, rinsed with deionized water and dried in air were used as a substrate. This procedure is used to remove organic and inorganic contamination from the substrate surface. Natural silicon oxide layer on the substrates was not removed. Before film sputtering, the substrates were heated during 4 h at 600°C with evacuation to $\sim 10^{-4}$ Pa.

CNW height was evaluated by the scribing trace profile made by a steel needle on the samples, CNW were completely removed in the scribing area. The scribing trace depth was measured by atomic-force microscopy using the Smena (NT-MDT) scanning probe microscope in atmosphere conditions by a semi-contact method.

Morphology of the sample surface was examined by scanning electron microscopy (SEM) using the Merlin (Carl Zeiss, Germany) electron microscope.

Raman scattering spectra (RSS) were measured on the Labram HR800 (HORIBA, France) spectrometer unit equipped with a confocal microscope. Exciting laser radiation at 532 nm was focused by the Olympus $100\times(NA = 0.9)$ objective into a spot with a diameter of $\sim 1\,\mu$m on the sample. Radiation power density on the sample surface was kept at lower than 2 kW/cm^2 to avoid the CNW structure degradation from laser radiation.

2. Findings and discussion

Analysis of SEM images of CNW deposited on the silicon substrates at the argon pressure of 3 Pa and HF power of 30 W with various deposition times (Figure 1, a–c) showed that CNW were formed in three steps.

CNW growth starts from island nuclei formation (Figure 1, a) and coalescence. Then CNW grows primarily in height (Figure 1, b). When CNW are higher than ~ 500 nm, CNW growth in height is followed by formation of „secondary“ graphene layers on side surfaces of CNW (Figure 1, c).

Dependences of CNW height on deposition time on the silicon substrate at the argon pressure of 3 Pa and HF power of 30 W are shown in Figure 2. Considerable influence of residual gases on the CNW growth on non-preheated substrates was observed at the island nucleation stage. Thus, CNW growth almost didn't take place during the first 20 min from the start of deposition (Figure 2, curve *2*).

Influence of residual gases on the carbon film sputtering rate was not observed (linear dependence of the film growth rate on time) during DC sputtering at the HF power of 60–200 W. Film growth on graphite coated substrates started without any delay. The rate of CNW nucleation on a graphite film and silicon substrate at high HF powers is probably higher than the graphite etching rate by residual gas atoms.

Morphology of CNW with the same height of 300 nm deposited in the same conditions (argon pressure 3 Pa, HF power 30 W) with and without substrate preheating appears to be different: CNW on a preheated substrate are arranged with a much higher density (amount of CNW per unit area) than CNW on a non-preheated substrate. This difference is probably explained by etching of CNW nucleus islands on the non-preheated substrate by residual gas molecule dissociation products. During substrate heating, surface-adsorbed residual atmospheric gas molecules are removed. These are mainly water vapor, nitrogen, oxygen, carbon dioxide, etc.

Ion bombardment of the growing structure surface by argon ions takes place during carbon film deposition by high-frequency magnetron graphite sputtering in argon plasma, as opposed to DC sputtering. Possibility of CNW growth proves that the ion bombardment intensity in high-frequency sputtering is sufficient for etching the amorphous phase of the film material.

Ion energy and flux are the ion bombardment intensity parameters. Their influence on the CNW formation and growth may be evaluated by review of the dependences of CNW morphology on HF power and argon pressure. Figure 1, d–g shows the SEM images of CNW about 500 nm in height deposited on silicon substrates at various

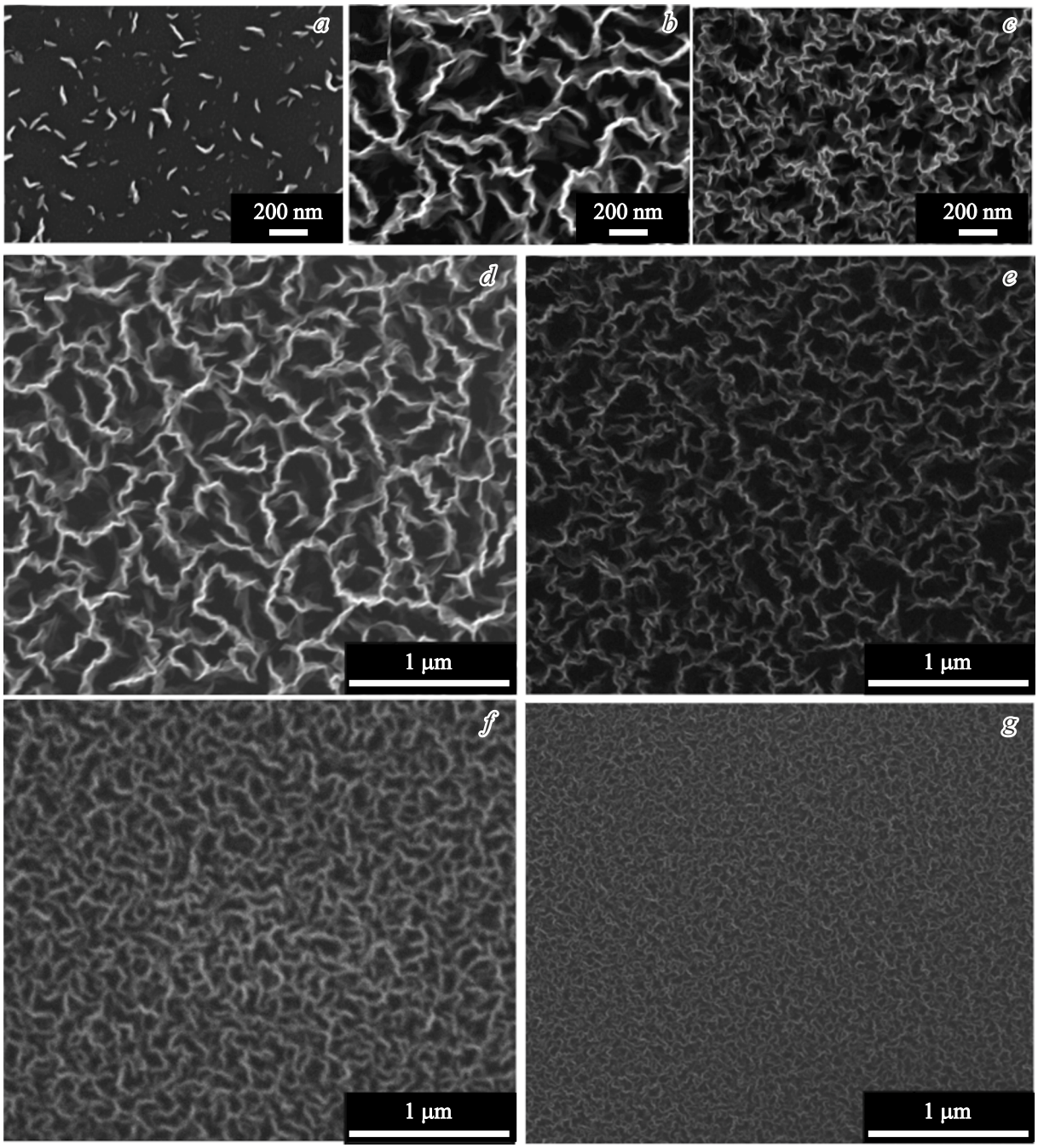

Figure 1. SEM images at various growth stages: *a* — sample № 5 (island nuclei, growth time 5 min), *b* — № 2 (CNW, growth time 60 min), *c* — № 3 (CNW, growth time 120 min). SEM images of CNW deposited at various HF power: *d* — № 2 (30 W), *e* — № 4 (65 W), *f* — № 6 (100 W), *g* — № 7 (160 W).

HF powers from 30 W to 160 W and argon pressure of 3 Pa. Comparative analysis of SEM images show that the CNW density grows with the increase in HF power. CNW thickness decreases from 40 nm at a HF power of 30 W to 8 nm at a HF power of 160 W. Increase in the CNW density and decrease in CNW thickness is especially pronounced when HF power increases from 100 W to 160 W.

Analysis of SEM images didn't detect any significant differences in the morphology of CNW samples deposited at the argon pressure from 1 Pa (minimum pressure at which glowing discharge may be ignited) to 7 Pa (pressure at which the film sputtering rate is maximum). Above 7 Pa, the effect of ion scattering on argon atoms starts and,consequently, the ion energy and ion flux attacking the growing film surface start decreasing.

Increase in the HF power leads to the growth of both the ion energy and flux. With plasma-forming gas pressure typical of magnetron sputtering, ion scattering is

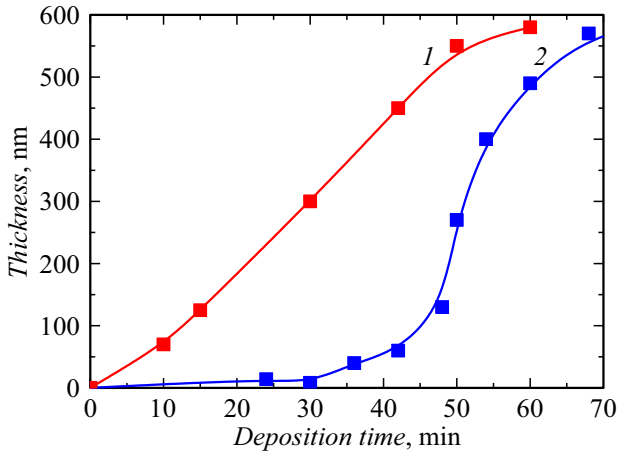

Figure 2. Dependence of CNW height on the sputtering time with substrate preheating (*1*) and without preheating (*2*).

insignificant. Therefore, the argon pressure doesn't affect the ion energy, and the ion flux, as well as the argon atom concentration, increases with pressure growth.

Comparison of the SEM data of CNW samples prepared with different intensity of ion bombardment of the growing film surface suggests that the increase in ion flux attacking the growing film surface doesn't cause significant changes in the SEM morphology, and the increase in HF power causes the increase in the CNW density on substrate.

Thin film deposition by magnetron target sputtering has particular restrictions. Increase in the plasma-forming gas pressure is higher than the pressure at which maximum film sputtering rate is observed, causes the decrease in ion energy and flux due to the increasing impact of ion flux scattering from plasma to the substrate on plasma-forming gas atoms. High HF power can give rise to target fracture and electrode sputtering.

Difference in the morphology of CNW deposited on the silicon substrates with uniform surface roughness max 2 nm and on substrates with longitudinal scratches 20–30 nm in depth remaining after mechanical polishing of the silicon substrate. In the latter case, CNW appeared to be oriented parallel to the scratches.

A sublayer with morphology similar to that of CNW was found on the SEM image of the film scribing trace. The sublayer was not damaged during scribing of the film. The sublayer probably has a hardness exceeding that of CNW. Typical height of island structural elements of the sublayer determined by the scanning probe microscopy is ~ 11 nm. The nature and structural properties of the sublayer have not been understood yet.

The presence of a sublayer under CNW was also noted by the authors of [17]. In their opinion, this was a „basal layer“ — several graphene layers. In [18], the authors reported that a 5 nm graphite sublayer was formed at the initial stage of CNW deposition in DC discharge in methane and hydrogen mixture without catalyst on the silicon substrate. During the film growth process, individual sublayer fragments grow, interact with each other and change their growth direction from horizontal to vertical in the electric field. However, these assumptions don't explain the specific morphology of the sublayer between the substrate and CNW. The absence of the „basal layer“ on a substrate with CNW made using a HF induction plasmatron by graphite ribbon sputtering in argon plasma without adding hydrogen and hydrocarbon radicals in the gas mixture was reported in [19]. In their opinion, this is associated with the features of CNW formation mechanisms at the initial growth stages using solid-state carbon sources.

Structural properties of CNW were studied by the RS spectroscopy method. RS spectra of the samples obtained at different values of pressure and power are shown in Figure 3. The experimental RS spectra contain lines referred in the literature as D, G, D', $D+D''$, $2D$, $D+D'$, respectively, in the frequency range 1350, 1581, 1620, 2450, 2690, 2940 cm^{-1}. The spectra are normalized to the amplitude of D-line. Line G in the graphene layer spectra is caused by scattering on an optical phonon with symmetry E_{2g} in the center of the Brillouin zone and is associated with planar vibrations of sp^2-hybridized carbon atoms in the graphene layer plane [20]. Line D results from resonance scattering of excited electrons on A_{1g} phonons and elastic scattering of these electrons on structural defects [20]. Structural defects of the lattice include breaking of the graphene lattice symmetry, for example, vacancies, dislocations or layer boundaries, inclusions of sp^3-hybridized carbon. Line D' is also associated with scattering processes involving crystal lattice defects [20,21].

Lines at $2200-3000\,\mathrm{cm}^{-1}$ are associated with two-phonon scattering processes. Small line $D+D''$ results from light scattering involving phonon superposition responsible for D- band and a longitudinal acoustic phonon at $1100\,\mathrm{cm}^{-1}$ [20]. Lines $2D$ and $2D'$ are overtones of lines D and D', respectively [20].

Structural properties of CNW were analyzed using the spectral data of RS lines. To determine positions, FWHM and line intensity, spectral profile was decomposed into individual lines (inset in Figure 3, *a*). The obtained numerical values of spectral characteristics of RS lines are listed in Table 2.

In the CNW RS spectrum, maximum of line G ($\nu(G)$) is in the high frequency region relative to the maximum position for bulk structurally perfect graphite $1581\,\mathrm{cm}^{-1}$. The observed high-frequency shift may be explained by compression strains that are probably caused by the curvature of graphene layers and also by structural defects.

Intensity ratio of lines D and G (I_D/I_G) characterized the degree of perfection of the graphene layer [21]. The lower I_D/I_G, the larger typical crystallite size is in the graphene basal plane. The crystallite may be represented as a region with size L_a bounded by linear defects [22]. The larger L_a, the lower linear defect concentration is. Point defects may be also present in graphene layers. Using the method developed in [22], values of L_a and $L_a$were determined. These values are listed in Table 2. For CNW formed at

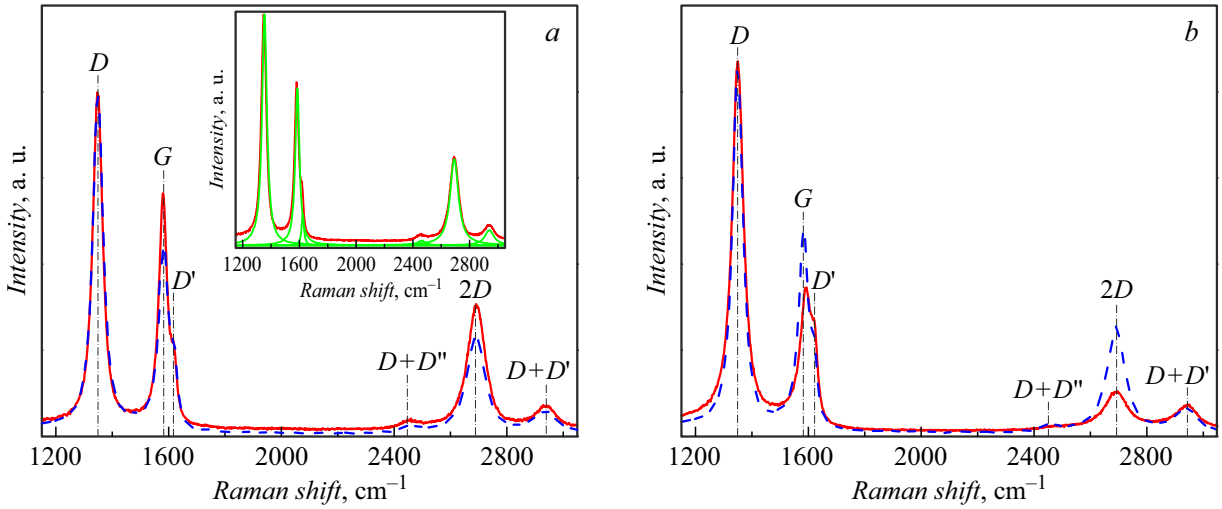

Figure 3. RS spectra of CNW obtained: *a* — at 3 Pa (dashed line, sample № 2) and 7 Pa (solid line, sample № 1), the inset shows the RS spectrum decomposition of sample № 1; *b* — at 30 W (dashed line, sample № 2) and 160 W (solid line, sample № 7).

Table 2. Spectral characteristics of CNW RS lines

Sample No.	$\nu(G)$,cm^{-1}	$\nu(D')$,cm^{-1}	FWHM(G), cm^{-1}	FWHM($2D$), cm^{-1}	I_D/I_G	I_{2D}/I_G	$I_D/I_{D'}$	L_a, L_d, nm
1	1581.3	1618.4	35.4	71.0	1.48	0.55	7.2	25.2, 7.2
2	1582.5	1619.3	40	75.8	1.9	0.54	6.9	20, 5.7
7	1590.3	1620.3	41.9	98.7	2.94	0.32	5.5	–

the HF power of 160 W (sample № 7), the model is not applicable due to high concentration of point defect.

Intensity ratio of lines $2D$ and G (I_{2D}/I_G) is used to determine the number of graphene monolayers in CNW (CNW thickness) [23]. Thus, the increase in the number of graphene layers is followed by the decrease in I_{2D}/I_G and increase in FWHM of line $2D$ [23,24]. For the prepared CNW, I_{2D}/I_G is within 0.32–0.55 and FWHM($2D$) is within 70–100 cm^{-1}, which corresponds to multilayer graphene with more than five layers.

Dependence of the intensity ratio of lines D and D' ($I_D/I_{D'}$) on the type of defects in the graphene layer is addressed in [25]. Analysis of various structural defects and RS spectra carried out by the authors of the paper showed $I_D/I'_D \sim 3.5$ for linear defects at the graphene crystallite interface, and $I_D/I_{D'} \sim 7$ for vacancy-type defects. For CNW samples studied in this work, $I_D/I_{D'}$ is within 5.5–7. This corresponds to a previous conclusion that point defects are the prevailing type of structural defects in all studied samples.

Increase in pressure from 3 Pa to 7 Pa is followed by the increase in L_a from 20 nm to 25 nm and L_d from 5.7 nm to 7 nm, which is indicative of the increase in the size of defect-free regions in CNW. However, $I_D/I_{D'}$ and I_{2D}/I_G remain almost unchanged, which indicates that vacancy type defects prevail and CNW thicknesses are unchanged.

Increase in the HF power from 30 W to 160 W give rise to the shift of line G in the RS spectra towards higher frequencies at ~ 8 cm^{-1} and increase in FWHM(G) at ~ 8 cm^{-1}. Increase in $I_D/I_{D'}$ to 5.5 with the increase in power indicates that the relative fraction of linear defects increases. As the HF power increases, the energy of growing CNW bombardment by argon ions increases leading to disordering of the graphene layer structure.

Conclusion

High-frequency magnetron graphite target sputtering was used to form CNW on polished KDB-10 (100) crystalline silicon substrates. CNW are formed in three stages — nucleation and coalescence; CNW growth mainly in height; after achievement of CNW height of about ~ 500 nm — CNW growth with formation of „secondary“ graphene layers on side surfaces of CNW. Substrate preheating considerably reduces the CNW nucleation and coalescence stage. Increase in the ion energy with the growth of HF power leads to the increase in CNW density on the substrate.

Analysis of the Raman scattering data showed that point defects are the prevailing type of structural defects in the prepared CNW. Increase in the HF power gives rise to the growth of structural defect concentration and, in particular, to a significant increase in the fraction of linear defects in

the CNW structure. On the other hand, argon pressure growth causes the increase in the size of defect-free regions on CNW.

Funding

The study was carried out using state budget funds for State Assignment FFUG-2024-0017.

Conflict of interest

The authors declare no conflict of interest.

References

[1] X. Zhao, H. Tian, M. Zhu, K. Tian, J.J. Wang, F. Kang, R.A. Outlaw. J. Power Sourc., **194** (2), 1208 (2009). DOI: 10.1016/j.jpowsour.2009.06.004
[2] Y.H. Wu, T. Yu, Z.X. Shen. J. Appl. Phys., **108**, 071301 (2010). DOI: 101063/1.3460809
[3] R. Vansweevelt, A. Malesevic, M. Van Gompel, A. Vanhulsel, S. Wenmackers, J. D'Haen. Chem. Phys. Lett., **485**, 196 (2010). DOI: 10.1016/j.cplett.2009.12.040
[4] D.A. Chernodubov, Yu.V. Bondareva, M.V. Shibalov, A.M. Mumlyakov, V.L. Zhdanov, M.A. Tarkhov, K.I. Maslakov, N.V. Suetin, D.G. Kvashnin, S.A. Evlashin. JETP Lett., **117** (6), 449 (2023). DOI: 10.1134/s0021364023600313
[5] A.I. Podlivaev, K.S. Grishakov, K.P. Katin, M.M. Maslov. JETP Lett., **114**, 143 (2021). DOI: 10.1134/S0021364021150078
[6] H.J. Cho, H. Kondo, K. Ishikawa, M. Sekine, M. Hiramatsu, M. Hori. Carbon, **68**, 380 (2014). DOI: 10.1016/j.carbon.2013.11.014
[7] L. Cui, J. Chen, B. Yang, D. Sun, T. Jiao. Appl. Surf. Sci., **357**, 1 (2015). DOI: 10.1016/j.apsusc.2015.08.252
[8] K. Bystrova, M.C.M. van de Sanden, C. Arnas, L. Marot, D. Mathys, F. Liu, L.K. Xu, X.B. Li, A.V. Shalpegin, G. De Temmerman. Carbon, **68**, 695 (2014). DOI: 10.1016/j.carbon.2013.11.051
[9] S. Seiji, H. Yuichi, T. Masanori, I. Takashi, N. Shuichi. Jpn. J. Appl. Phys., **47**, 8635 (2008). DOI: 10.1143/JJAP.47.8635
[10] J. Yang, Q. Yang, Y. Zhang, X. Wei, H. Shi. RSC Adv., **13** (33), 22838 (2023). DOI: 10.1039/d3ra03104g
[11] A.M. Mumlyakov, E.A. Pershina, A.A. Shibalova, M.V. Shibalov, Yu.V. Anufriev, I.A. Filippov, V. Sen', M.A. Tarkhov. St. Petersburg State Polytech. Univ. J.: Phys. Math., **16**, 211 (2023). DOI: 10.18721/JPM.163.236
[12] Y. Yerlanuly, D. Christy, N. Van Nong, H. Kondo, B. Alpysbayeva, R. Nemkayeva, M. Kadyr, T. Ramazanov, M. Gabdullin, D. Batryshev, M. Hori. Appl. Surf. Sci., **523**, 146533 (2020). DOI: 10.1016/j.apsusc.2020.146533
[13] S.A. Grudinkin, A.Ya. Vinogradov. J. Phys.: Conf. Series, **1697**, 012108 (2020). DOI: 10.1088/1742-6596/1697/1/012108
[14] F. Guzman-Olivos, R. Espinoza-Gonzalez, V. Fuenzalida. Mater. Lett., **167**, 242 (2016). DOI: 10.1016/j.matlet.2016.01.016
[15] E.S. Tuzemen, M. Kilic, B.K. Zeyrek, A.E. Kasapoglu, E. Gur, B.O. Alaydin, M. Esen, R. Esen. Diam. Relat. Mater., **93**, 200 (2019). DOI: 10.1016/j.diamond.2019.02.007
[16] T. Itoh. Thin Solid Films, **519**, 4589 (2011). DOI: 10.1016/j.tsf.2011.01.308
[17] W. Zheng, X. Zhao, W. Fa. Appl. Mater. Interfaces, **13**, 9561 (2021). DOI: 10.1021/acsami.0c19188
[18] V.A. Krivchenko, V.V. Dvorkin, N.N. Dzbanovsky, M.A. Timofeyev, A.S. Stepanov, A.T. Rakhimov, N.V. Suetin, O.Yu. Vilkov, L.V. Yashina. Carbon, **50**, 1477 (2012). DOI: 10.1016/j.carbon.2011.11.018
[19] W. Fu, X. Zhao, W. Zheng. Carbon, **173**, 91 (2021). DOI: 10.1016/j.carbon.2020.10.072
[20] A.C. Ferrari, D.M. Basko. Nature Nanotech., **8** (4), 235 (2013). DOI: 10.1038/nnano.2013.46
[21] L.G. Cançado, K. Takai, T. Enoki, M. Endo, Y.A. Kim, H. Mizusaki, A. Jorio, L.N. Coelho, R. Magalhães-Paniago, M.A. Pimenta. Appl. Phys. Lett., **88** (16), 163106 (2006). DOI: 10.1063/1.2196057
[22] L.G. Cançado, M.G. Da Silva, E.H.M. Ferreira, F. Hof, K. Kampioti, K. Huang, A. Pénicaud, C.A. Achete, R.B. Capaz, A. Jorio. 2D Materials, **4** (2), 025039 (2017). DOI: 10.1088/2053-1583/aa5e77
[23] E. Bertran-Serra, A. Musheghyan-Avetisyan, S. Chaitoglou, R. Amade-Rovira, I. Alshaikh, F. Pantoja-Suárez, J.-L. Andújar-Bella, T. Jawhari, A. Perez-del-Pino, E. Gyorgy. Appl. Surf. Sci., **610**, 155530 (2023). DOI: 10.1016/j.apsusc.2022.155530
[24] Y. Hao, Y. Wang, L. Wang, Z. Ni, Z. Wang, R. Wang, C.K. Koo, Z. Shen, J.T. Thong. Small, **6** (2), 195 (2010). DOI: 10.1002/smll.200901173
[25] A. Eckmann, A. Felten, A. Mishchenko, L. Britnell, R. Krupke, K.S. Novoselov, C. Casiraghi. Nano Lett., **12** (8), 3925 (2012). DOI: 10.1021/nl300901a

Translated by E.Ilinskaya